IEEE Access
Multidisciplinary | Rapid Review | Open Access Journal

Received July 31, 2019, accepted August 16, 2019, date of publication August 28, 2019, date of current version September 12, 2019.

Digital Object Identifier 10.1109/ACCESS.2019.2937987

A Triple Band Hybrid MIMO Rectangular Dielectric Resonator Antenna for LTE Applications

IRENE KONG CHEH LIN[1], MOHD HAIZAL JAMALUDDIN[1], (Member, IEEE), AZLAN AWANG[2], (Senior Member, IEEE), RAGHURAMAN SELVARAJU[1], MUHAMMAD HASHIM DAHRI[3], LEOW CHEE YEN[1], (Member, IEEE), AND HASLIZA A. RAHIM[4], (Member, IEEE)

[1]Wireless Communication Centre, School of Electrical Engineering, Universiti Teknologi Malaysia, Johor Bahru 81310, Malaysia
[2]Department of Electrical and Electronic Engineering, Universiti Teknologi PETRONAS, Seri Iskandar 32610, Malaysia
[3]Faculty of Electrical and Electronic Engineering, Universiti Tun Hussein Onn Malaysia, Parit Raja 86400, Malaysia
[4]Bioelectromagnetic Research Group, School of Computer and Communication Engineering, Universiti Malaysia Perlis, Arau 02600, Malaysia

Corresponding author: Mohd Haizal Jamaluddin (haizal@fke.utm.my)

This work was supported in part by the Universiti Teknologi Malaysia under TDR Grant vote 05G20 and in part by the Universiti Teknologi PETRONAS under Grant vote 4B308.

ABSTRACT In this paper, a triple band Multiple-Input Multiple-Output (MIMO) Rectangular Dielectric Resonator Antenna (RDRA) designed using hybrid techniques for Long Term Evolution (LTE) applications is investigated and presented. The proposed MIMO antenna can transmit and receive data independently by covering LTE Band 8 at 0.9 GHz, LTE Band 3 at 1.8 GHz, and LTE Band 40 at 2.3 GHz. Hybrid technique is adopted in this design by combining a meander line antenna with an RDRA to realize multiband operation. Meander line antenna has been proposed over the long vertical microstrip feeding line at 0.9 GHz, to employ a size reduction in the antenna, while two modes of RDRA are applied in this design: $TE^{y}_{1\delta1}$ mode at 1.8 GHz and $TE^{y}_{2\delta1}$ mode at 2.3 GHz. The proposed MIMO antenna has been fabricated and experimentally tested. The measured impedance bandwidths (S_{11}<-10 dB) for the three stated bands are 4.40%, 11.36%, and 2.54% at Port 1, respectively and 5.47%, 10.54%, and 3.43% at Port 2, respectively. Measured isolations of −15.3 dB, −17.8 dB, and −47.0 dB are obtained at each described frequency, respectively. The performance of the proposed MIMO antenna is further validated using over-the-air LTE downlink throughput test. Throughputs of 93.16 Mbps, 93.01 Mbps, and 87.30 Mbps have been achieved for 0.9 GHz, 1.8 GHz, and 2.3 GHz, respectively, using 64 Quadrature Amplitude Modulation (QAM). In this regard, it is conceived that the proposed MIMO antenna can be a good candidate for LTE applications due to the validated excellent throughput performance.

INDEX TERMS Hybrid technique, LTE, meander line, MIMO, rectangular DRA, throughput.

I. INTRODUCTION

The present mobile communication technology, Long Term Evolution (LTE), is widely used in mobile devices such as smartphones, laptops, and tablets due to its high spectrum efficiency, high speed transmission, and high data rates [1]. The operating frequency of LTE ranges from 400 MHz to 4 GHz [2]. A small size multiband MIMO antenna designed with high isolation is preferable for LTE applications [3].

Multiple-Input Multiple-Output (MIMO) technology has been developed to provide excellent channel capacity and high data rates in wireless communications [4]. It is implemented by utilizing multiple antennas at the transmitting and receiving ends of the communication system to combat multipath fading [5], resulting in improved channel capacity and data rates [1]. The MIMO technology is launched either in a parallel or orthogonal mode excitation scheme [6]. For parallel configuration, the feeding ports are fed by the same feeding techniques. Such configurations are shown by the two bent meander line antennas [7] and two identical meander line antennas [8], where both of them are placed along the same *x*-axis. For orthogonal configuration, the perpendicular feeding ports can be fed by the same or different feeding techniques. The former shows that an L-shaped DRA is excited by two symmetrical slots of equal dimensions coupled through microstrip feed lines in [9]. Meanwhile,

The associate editor coordinating the review of this article and approving it for publication was Chuan Huang.

an RDRA that is excited with two feeding techniques: a coplanar waveguide (CPW) inductive slot for Port 1 and a coaxial probe for Port 2 in [1], is depicted by the latter. Despite that, there are also two RDRAs utilized in orthogonal MIMO design. In [6], two DRAs that are excited by two coplanar waveguides (CPW), are compared in terms of the space between two elements of the antenna, and isolation for orthogonal and parallel configurations. As reported in [6], two antennas that were separated by 3.75 mm in an orthogonal configuration managed to produce −27 dB of isolation, compared to the two antennas which were separated by 118 mm in a parallel configuration with an isolation of −20 dB only. The orthogonal configuration in [6] shows that the size of the MIMO system is significantly reduced and high isolation between the two antenna ports is achieved [2]. However, the design of the orthogonal antennas in [6] would be more complicated if one DRA was shared between the two perpendicular feeding ports.

The major challenge in the design of a MIMO antenna is the existence of an undesirable mutual coupling effect [10], [11] as higher mutual coupling has an adverse effect on the channel capacity [12], [13]. Meanwhile, the capacity of the MIMO system is the highest among the other systems, namely SISO (Single-Input Single-Output), SIMO (Single-Input Multiple-Output), and MISO (Multiple-Input Single-Output) due to the presence of a greater number of antennas at the transmitter and receiver sides [14]. As reported in [9], by using 64 QAM, about 93.152 Mbps of the measured throughput of the MIMO system is obtained, which is almost twice that of 50.190 Mbps, the SISO system at 1.8 GHz. Therefore, the maximum data rates can be acquired by having high isolation of MIMO antennas.

As compared to microstrip antennas, DRAs are widely used in the electromagnetic field due to their superior characteristics such as low metallic losses, high efficiency, high gain at high frequencies [15], [16], flexibility in their shapes and excitation mechanisms [6]. Additionally, DRAs provide a wider impedance bandwidth [15]. A microstrip antenna radiates through two narrow radiation slots, whereas DRA radiates through the entire DRA surface except for the grounded part [17]. Meanwhile, meander line antenna has been proposed in [7], [8] and [18] to achieve a size reduction in the antenna instead of having the long vertical microstrip feeding line.

In the recent era of wireless communication, a multiband antenna is desirable because each nation or wireless carrier uses different frequency bands [19]. Different techniques such as higher order mode generation in DRA [20], combination of DRA with parasitic element (not directly connected to feeding structure) [21] and combination of DRA with other radiating structures (directly connected to feeding structure) [22] are used to realize multiband operation. Nevertheless, hybrid techniques where DRA combines with other radiating structures [22] such as Defected Ground Structure (DGS) [23], triangular-shaped microstrip line [24], ring slot [25], trapezoidal patch microstrip feed [26] and folded microstrip line [22], are discussed in this paper. The antenna in [22], which is designed with the MIMO system, is superior to single port antennas that have been proposed in [23]–[26]. To the best of the authors' knowledge, none of the previous work utilized the meander line merging with DRA resonating at three distinct LTE frequencies for identical MIMO antenna.

In this paper, a triple band rectangular DRA designed with two ports using hybrid technique for LTE applications is proposed. The hybrid technique consists of a meander line antenna and an RDRA, where the meander line antenna, fundamental $TE^{y}_{1\delta1}$ mode and $TE^{y}_{2\delta1}$ mode of RDRA resonate at 0.9 GHz, 1.8 GHz, and 2.3 GHz, respectively, for LTE applications. A rectangular shape is chosen because it provides one more degree of freedom than cylindrical DRAs and hemispherical DRAs [17], which can be used to control impedance bandwidth by adjusting the ratios of length-height and width-height [27]. Simulation of the presented MIMO antenna is performed with Ansys HFSS (High Frequency Structure Simulator) version 2019. Reference levels on return loss for impedance bandwidth and isolation are −10 dB and −15 dB, respectively, in this research work.

This paper is organized as follows. In Section II, geometries of single port and MIMO hybrid DRAs are presented, followed by their parametric studies. In the meantime, Section III presents the fabricated single port and MIMO antennas. Their measured antenna parameters are compared to the simulation results. Furthermore, MIMO performance of the proposed MIMO antenna is assessed, followed by the comparison analysis between the proposed MIMO antenna and existing structures. Finally, Section IV concludes the discussion of this paper.

II. ANTENNA DESIGN AND ANALYSIS

This section presents the geometries of a single port and MIMO hybrid DRAs. For single port design, a parametric study of the vertical position of DRA is performed. Meanwhile, for MIMO design, parametric studies of the separation length between two ports are investigated based on identical and non-identical designs.

A. SINGLE PORT HYBRID DRA

Fig. 1a shows the geometry of a single port hybrid DRA. A rectangular dielectric resonator (DR) antenna and a meander line are coupled through 50Ω microstrip feed line on $90[L] \times 45[WG]$ mm^2 of FR4 substrate ($\varepsilon_r = 4.6$) with a thickness of 1.6 mm. The DRA's dimensions for the fundamental $TE^{y}_{1\delta1}$ mode are calculated using Equations (1) to (5) [17]:

$$k_x = \frac{\pi}{a} \tag{1}$$

$$k_z = \frac{\pi}{d} \tag{2}$$

$$k_y tan\frac{(k_y b)}{2} = \sqrt{(\varepsilon_r - 1)k_0{}^2 - k_x{}^2} \tag{3}$$

$$k_x^2 + k_y^2 + k_z^2 = \varepsilon_r k_o^2 \tag{4}$$

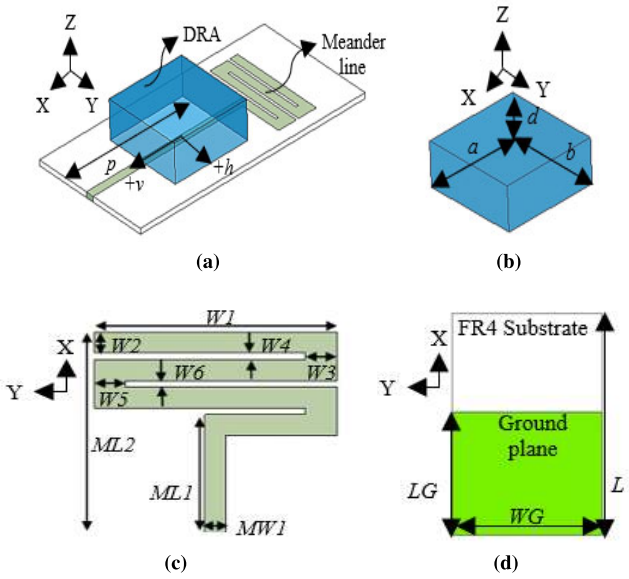

FIGURE 1. Single port hybrid DRA geometry (a) Overall 3D view (b) 3D view of DRA (c) Front view without DRA (d) Back view.

TABLE 1. Optimized design parameters.

Parameter	Value (mm)	Parameter	Value (mm)
a	29	$W2$	3
b	29	$W3$	4.5
d	11.4	$W4$	1
h	0	$W5$	4.5
L	90	$W6$	1
p	50.2	LG	50
v	9.3	WG	45
W	107.8	$ML1$	62.9
Y	62.8	$MW1$	3
$W1$	35	$ML2$	74.9

$$k_0 = \frac{2\pi f_r}{c} \tag{5}$$

where k_x, k_y, k_z are the wave numbers in the x-, y- and z-axes, k_0 is the free-space wave number, f_r is the resonant frequency and c is the speed of light in free space. Fig. 1b illustrates that the volume of DRA at 1.8 GHz is $29[a]\times29[b]\times11.4[d]\ mm^3$ with relative permittivity (ε_r) of 30 and loss tangent (tan δ) of 0.019. Meanwhile, the meander line which is resonating at 0.9 GHz, has an overall feeding length *(ML2)* of 74.9 mm, feeding width *(MW1)* of 3 mm, width *(W1)* of 35 mm, and length ($W2$) of 3 mm, as depicted in Fig. 1c. The same left and right widths ($W3$ and $W5$) and gaps ($W2$ and $W4$) of the meander-line antenna are 4.5 mm and 1 mm, respectively. Copper with a thickness of 35 μm is cladded on the front and back sides of the substrate plane, as shown in Fig. 1c and Fig. 1d, respectively. In this work, $50[LG]\times45[WG]\ mm^2$ of a partial ground plane is used instead of full ground because it gives the widest impedance bandwidth at 1.8 GHz. Table 1 lists the optimized design parameters after the parametric analysis.

To verify the proposed hybrid technique, E-field distributions of the single port antenna at the three mentioned

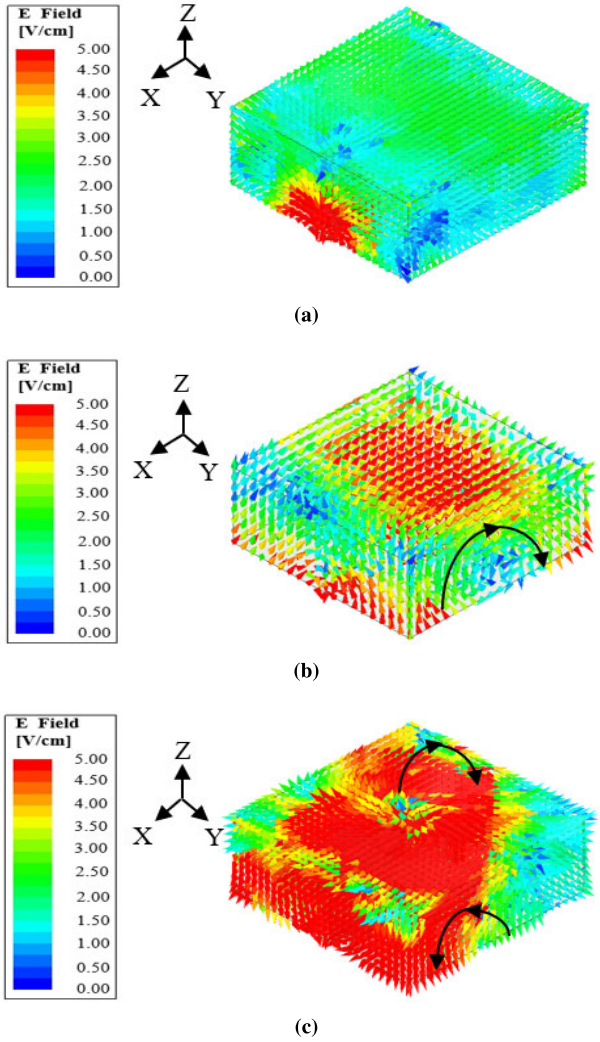

FIGURE 2. E-field distributions at different frequencies (a) 0.9 GHz (b) 1.8 GHz (c) 2.3 GHz.

frequencies are evaluated and presented in Fig. 2. With reference to Fig. 2, the red region indicates the strongest electric field, whereas the blue area denotes the weakest electric field. From Fig. 2a, it is clearly noticed that the maximum electric field lies at the bottom of DRA. Since the meander line is designed at 0.9 GHz, therefore, there must be no circular movement of the electric field inside the DRA. Meanwhile, Fig. 2b demonstrates that one half cycle of electric fields circulate around the y-axis and vary in x- and z-axes inside the DRA at 1.8 GHz. Consequently, it proves successfully that the fundamental resonant mode of DRA at 1.8 GHz is $TE^{y}_{1\delta1}$. Other than that, the second resonant mode of the DRA in this research work is $TE^{y}_{2\delta1}$, as electric fields vary in two half cycles with variation along x-axis inside the DRA at 2.3 GHz, as shown in Fig. 2c.

In order to achieve optimal performance, a parametric study is performed on the vertical position of DRA (v) from 0 mm to 12 mm, to determine its effect on return loss (S_{11}) for single port hybrid DRA, as shown in Fig. 3. Initially, the DRA

is placed at the center ($v = 0$ mm) on the 90×45 mm^2 of the substrate plane. In this case, the bandwidth performance at 1.8 GHz is not convincing since the microstrip feed line is designed at 0.9 GHz. Therefore, it can be observed that when the DRA moves downward, the bandwidth at 1.8 GHz gets wider. It is because the fundamental resonance of DRA gets closer to 50Ω of impedance matching at 1.8 GHz, based on the design of microstrip feeding line at 0.9 GHz. However, the return loss at 2.3 GHz is not affected since it is the second resonance frequency of DRA. As illustrated in Fig. 3, the two possible candidates of v are 9.3 mm and 12 mm, where the single port hybrid DRA is able to have less than -10 dB of return loss at the three aforementioned bands respectively. Despite that, the bandwidth at 1.8 GHz decreases with additional unwanted resonant frequency at 1.5 GHz when $v =$ 12 mm. Therefore, for single port hybrid DRA, the optimal value of the vertical position of DRA is 9.3 mm.

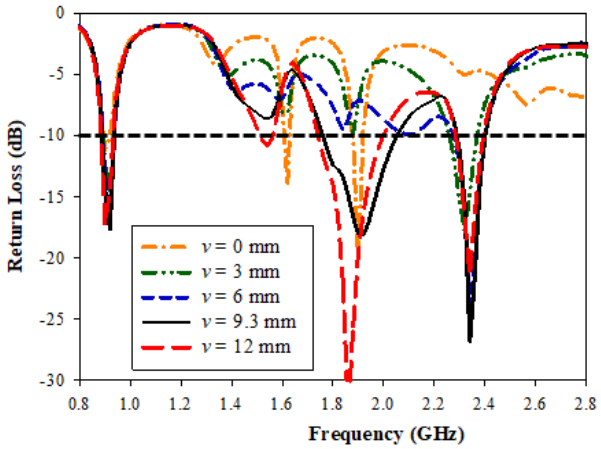

FIGURE 3. Simulated return loss (S_{11}) for different values of DRA's vertical position (v) in single port design.

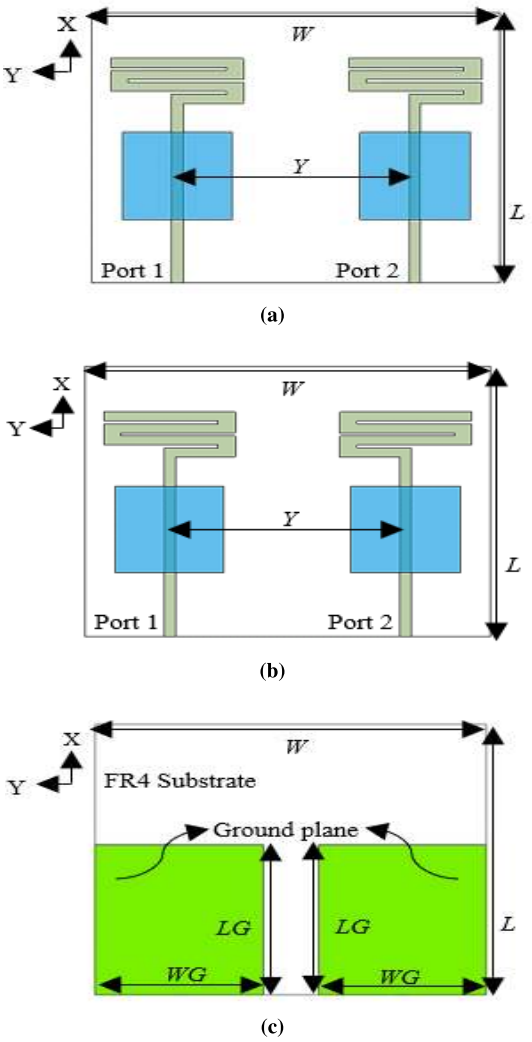

FIGURE 4. MIMO hybrid DRA geometry (a) Identical MIMO design in front view (b) Non-identical MIMO design in front view (c) Back view.

B. MIMO HYBRID DRA

In order to increase channel capacity and data rates, which are highly demanded by users, the MIMO technology is implemented. In this work, a parallel excitation scheme is used by duplicating a single port hybrid DRA with a separation length between two ports *(Y)* along the *y*-axis, as shown in Fig. 4. There are two cases for MIMO designs, namely identical and non-identical designs. All parameters are kept constant except for the placement of two meander lines. An identical MIMO design is categorized by putting two symmetrical meander lines together along the *y*-axis, as shown in Fig. 4a. Meanwhile, a non-identical MIMO design is classified and displayed in Fig. 4b, which is due to the placement of two asymmetrical meander lines along the *y*-axis. The front views of identical and non-identical MIMO designs are illustrated in Fig. 4a and Fig. 4b, respectively. Both identical and non-identical MIMO designs use the same back view, as displayed in Fig. 4c.

For both identical and non-identical MIMO designs, a parametric study on the separation length between two ports *(Y)* is performed from 60.8 mm to 65.8 mm, where 65.2 mm is $0.5\lambda_0$ for 2.3 GHz. Tables 2 and 3 demonstrate the effects of Y on covered impedance bandwidths and gains for Ports 1 and 2, and also isolation in identical and non-identical MIMO designs, respectively. Since S_{21} has the same isolation value as S_{12}, only S_{12} is stated in this research work. In fact, the antenna is considered to cover the essential downlink bandwidth at 0.9 GHz if the end of impedance bandwidth is beyond 0.925 GHz. It is apparent that Y has a dominant effect on the covered downlink bandwidth (0.925-0.960 GHz) and isolation at 0.9 GHz, due to the placement of two meander lines based on the observations from Tables 2 and 3. Nevertheless, the effects of Y are negligible at 1.8 GHz and 2.3 GHz. Therefore, Y is a prominent parameter in determining the covered downlink bandwidth and isolation, especially at 0.9 GHz, in this work.

For the identical MIMO design, the effects of Y on input return loss (S_{11}) and isolation (S_{12}) are displayed in Fig. 5 and Fig. 6, respectively. Table 2 has been referred to, such that, the covered downlink bandwidth at 0.9 GHz for

TABLE 2. Simulated antenna parameters for different values of the separation length between two ports (*Y*) in identical MIMO design.

Antenna Parameters		Freq. (GHz)	*Y* (mm) 60.8	61.8	62.8 (Nominal)	63.8	64.8	65.8
Covered BW. (GHz)	Port 1	0.9	0.86 - 0.92	0.88 - 0.93	0.89 - 0.93	0.90 - 0.91	0.88 - 0.93	0.90 - 0.94
		1.8	1.74 - 2.09	1.73 - 2.09	1.73 - 2.09	1.74 - 2.08	1.74 - 2.08	1.75 - 2.08
		2.3	2.29 - 2.40	2.29 - 2.40	2.29 - 2.40	2.29 - 2.40	2.29 - 2.40	2.29 - 2.40
	Port 2	0.9	0.86 - 0.92	0.87 - 0.92	0.89 - 0.94	0.90 - 0.92	0.88 - 0.93	0.89 - 0.94
		1.8	1.75 - 2.08	1.75 - 2.08	1.74 - 2.07	1.75 - 2.07	1.75 - 2.07	1.75 - 2.07
		2.3	2.31 - 2.40	2.30 - 2.40	2.30 - 2.40	2.30 - 2.40	2.30 - 2.40	2.30 - 2.40
Isolation (dB)		0.9	-7.0	-10.2	-17.5	-9.1	-12.4	-21.4
		1.8	-16.9	-16.8	-16.9	-17.2	-17.0	-17.4
		2.3	-27.2	-27.7	-28.5	-29.0	-29.2	-29.6
Gain (dBi)	Port 1	0.9	4.1	4.1	4.1	4.1	4.1	4.1
		1.8	4.0	4.0	4.2	4.3	4.4	4.4
		2.3	1.2	1.0	1.4	1.1	1.2	1.0
	Port 2	0.9	4.1	4.1	4.1	4.1	4.1	4.1
		1.8	3.9	3.9	4.0	4.1	4.1	4.1
		2.3	1.9	2.1	2.0	2.0	1.9	2.0

TABLE 3. Simulated antenna parameters for different values of the separation length between two ports (*Y*) in non-identical MIMO design.

Antenna Parameters		Freq. (GHz)	*Y* (mm) 60.8	61.8	62.8	63.8 (Nominal)	64.8	65.8
Covered BW. (GHz)	Port 1	0.9	0.89 - 0.93	0.84 - 0.91	0.84 - 0.90	0.89 - 0.95	-	0.88 - 0.93
		1.8	1.71 - 2.09	1.72 - 2.09	1.71 - 2.09	1.72 - 2.09	1.73 - 2.08	1.73 - 2.08
		2.3	2.29 - 2.40	2.29 - 2.40	2.30 - 2.40	2.29 - 2.40	2.29 - 2.40	2.29 - 2.40
	Port 2	0.9	0.87 - 0.93	0.86 - 0.92	0.87 - 0.90	0.90 - 0.95	-	0.87 - 0.93
		1.8	1.71 - 2.09	1.71 - 2.09	1.72 - 2.09	1.71 - 2.08	1.72 - 2.08	1.73 - 2.08
		2.3	2.29 - 2.40	2.29 - 2.40	2.30 - 2.40	2.29 - 2.40	2.29 - 2.40	2.29 - 2.40
Isolation (dB)		0.9	-8.8	-8.6	-9.9	-24.4	-7.1	-12.5
		1.8	-16.0	-16.2	-16.2	-16.4	-16.8	-17.1
		2.3	-20.2	-20.5	-18.9	-21.2	-21.5	-22.2
Gain (dBi)	Port 1	0.9	4.0	3.9	4.0	4.0	3.9	3.9
		1.8	3.5	3.7	3.8	3.8	4.0	3.7
		2.3	0.4	0.8	0.9	0.9	0.8	0.8
	Port 2	0.9	4.0	4.0	4.0	3.9	3.9	4.0
		1.8	3.6	3.7	4.0	3.9	4.0	3.9
		2.3	0.8	1.0	0.8	0.9	0.9	0.6

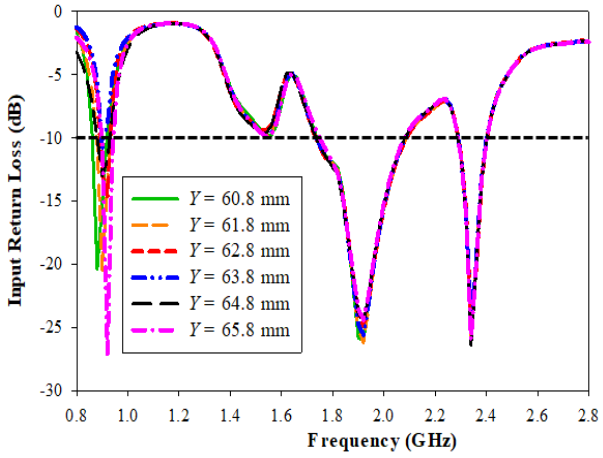

FIGURE 5. Simulated input return loss (S_{11}) for different values of the separation length between two ports (*Y*) in identical MIMO design.

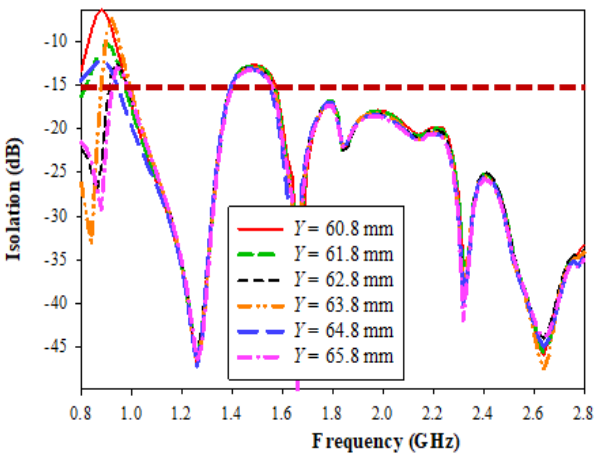

FIGURE 6. Simulated isolation (S_{12}) for different values of the separation length between two ports (*Y*) in identical MIMO design.

Port 1 is difficult to be determined from Fig. 5. Based on the tabulated impedance bandwidths at Port 1 in Table 2, the possible candidates of *Y* are 61.8 mm, 62.8 mm, 64.8 mm, and 65.8 mm, since each of them has beyond 0.925 GHz at the end of impedance bandwidth at Port 1, indicating that the MIMO antenna has covered essential downlink bandwidth at 0.9 GHz.

The four possible candidates of *Y* for identical MIMO design are further evaluated by isolation of −15 dB in this work. With reference to Fig. 6, it is obvious that the isolation

improved with increment in Y when started with 60.8 mm. Despite that, when Y reached 63.8 mm, the isolation was found to be dropped at −9.1 dB and after that, the isolation improved again with the increment in Y. Among the four possible candidates of Y which have been mentioned previously, 61.8 mm and 64.8 mm of Y are eliminated since their isolation values are greater than −15 dB. Therefore, for identical MIMO design, 62.8 mm of Y is opted due to the main reason of having shorter separation length than 65.8 mm, although 65.8 mm has the least undesirable isolation. Meanwhile, for non-identical MIMO design, 63.8 mm of Y is selected since it is the only candidate that has less than −15 dB of isolation and covers downlink bandwidth at 0.9 GHz based on the tabulated results in Table 3.

Both, $Y = 62.8$ mm in identical MIMO design and $Y = 63.8$ mm in non-identical MIMO design manage to cover the downlink bandwidth and pass the isolation requirement, particularly at 0.9 GHz. However, by referring to the values of gain that are tabulated in Tables 2 and 3, identical MIMO design is preferred, as its higher gain at the three described frequencies far outweigh its greater undesirable isolation. All gains at both ports in identical MIMO design are higher than non-identical MIMO design, especially at 2.3 GHz for Port 2. The former, which has 2.0 dB of gain, is approximately twice of 0.9 dB to the latter. Therefore, the overall volume of the proposed identical MIMO antenna in this research work is $107.8[W] \times 90[L] \times 11.4[d]\ mm^3$, as depicted in Fig. 4a.

III. RESULTS AND DISCUSSIONS

This section presents the fabricated prototypes, measurement procedures and the corresponding results of the single port antenna and the proposed MIMO hybrid DRA. Agilent E5071C ENA Network Analyzer is utilized to measure their S-parameters. Simulated gains, radiation efficiencies, and radiation patterns at each described frequency are compared with measurements that have been conducted inside the NSI anechoic chamber. Additionally, MIMO performances such as Envelope Correlation Coefficient (ECC), Diversity Gain (DG), Mean Effective Gain (MEG) and Total Active Reflection Coefficient (TARC) are calculated and analyzed based on the simulated and measured S-parameters. Furthermore, the theoretical maximum and the actual average measured throughput of SISO and 2 × 2 MIMO systems for the three modulation schemes are obtained at each mentioned frequency using an over-the-air LTE downlink throughput test.

A. ANTENNA PARAMETERS ANALYSIS FOR SINGLE PORT HYBRID DRA

The DR is fabricated with the ECCOSTOCK HiK dielectric material ($\varepsilon_r = 30$) while the meander line and the ground plane are fabricated by etching the FR4 substrate ($\varepsilon_r = 4.6$). They are excited through a 3.5 mm 50Ω SMA connector. Fabricated prototype of the single port hybrid antenna is displayed in Fig. 7.

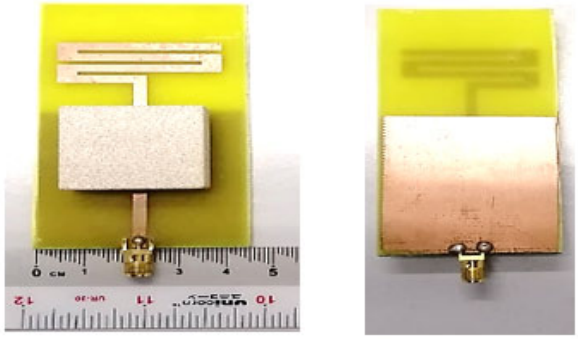

FIGURE 7. Prototype of the single port hybrid DRA (a) 3D view (b) Back view.

The fabricated single port hybrid RDRA antenna is connected to Port 1 of the network analyzer using a coaxial cable for S-parameter measurement performance. A comparison between the simulated and measured S-parameters is presented in Fig. 8, by having a reference level of −10 dB on S_{11} for impedance bandwidth. As indicated in Fig. 8, 12.66% (1.78-2.02 GHz) of the measured impedance bandwidth at 1.8 GHz obviously differs from the simulation, 15.27% (1.76-2.05 GHz). However, the prototype shows a good match at 0.9 GHz and 2.3 GHz. The simulated and measured impedance bandwidths are 5.47% (0.89-0.94 GHz) and 4.40% (0.89-0.93 GHz) at 0.9 GHz, respectively, whereas 4.69% (2.29-2.40 GHz) and 2.99% (2.31-2.38 GHz) at 2.3 GHz, respectively. Each simulated and measured antenna parameter has been compared and tabulated in Table 4. Based on the observations from Table 4, the simulated and measured values of gain and radiation efficiency within the bands of interest are similar.

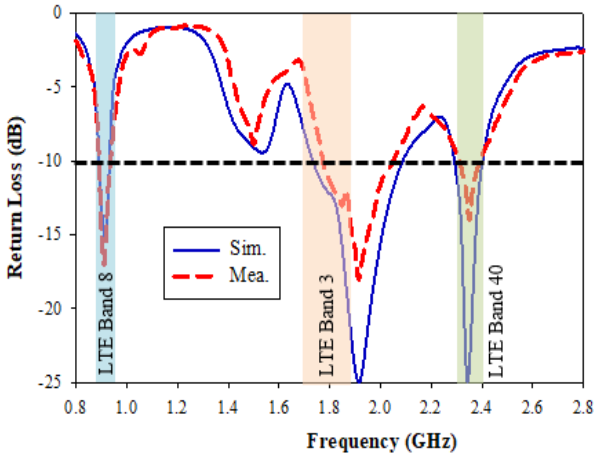

FIGURE 8. Simulated and measured return loss (S_{11}) of the single port hybrid DRA.

E-plane and H-plane views of the measured and simulated normalized radiation patterns are collectively displayed in Fig. 9, by following the sequence of described frequen-

TABLE 4. Comparison between simulation and measurement of each antenna parameter for single port hybrid DRA.

Antenna Parameters		Freq. (GHz) 0.9	1.8	2.3
Covered BW. (%)	Sim.	5.47	15.27	4.69
	Mea.	4.40	12.66	2.99
Gain (dBi)	Sim.	1.4	3.9	0.2
	Mea.	1.3	3.7	0.2
Rad. Eff. (%)	Sim.	84	75	60
	Mea.	80	70	55

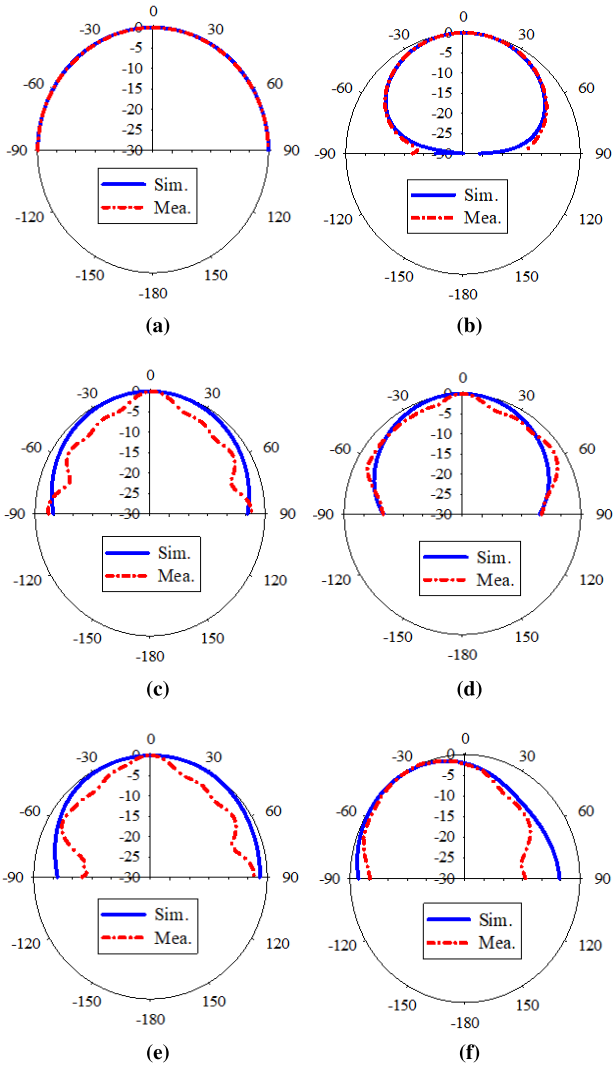

FIGURE 9. Measured and simulated normalized radiation patterns of the single port hybrid DRA (a) E-Plane at 0.9 GHz (b) H-Plane at 0.9 GHz (c) E-Plane at 1.8 GHz (d) H-Plane at 1.8 GHz (e) E-Plane at 2.3 GHz (f) H-Plane at 2.3 GHz.

cies. As indicated in Fig. 9, all normalized radiation patterns point in broadside directions at the three frequencies, except Fig. 9f, which points in −45° for H-plane at 2.3 GHz. Nevertheless, there are some apparent differences between simulated and measured normalized radiation patterns, especially at 1.8 GHz, as shown in both Fig. 9c and Fig. 9d. The first potential cause of this difference is the imperfect size of the fabricated DRA. Some tiny fragments on the DRA were found missing during the fabrication process due to its increased affinity towards ceramic material when its permittivity exceeds 10. Additionally, a double tape was used to mount the DRA at its designated vertical position in this work. Consequently, there are some possibilities of air gaps between the surface of the DRA and the FR4 substrate, causing extra permittivity which degrades the performance of the return loss at 1.8 GHz. Furthermore, the placement of the fabricated DRA on its designated vertical position is critical, as tolerance of a few millimeters will give a smaller bandwidth response at 1.8 GHz, as shown in Fig. 2. Hence, by improving these tolerances, the performance in return loss and radiation patterns at 1.8 GHz for single port hybrid DRA can be closer to the simulation results.

B. ANTENNA PARAMETERS ANALYSIS FOR MIMO HYBRID DRA

The proposed MIMO antenna with optimal parameters is fabricated and displayed in Fig. 10. The left SMA connector of the MIMO prototype is recognized as Port 1, whereas the right SMA connector of the MIMO prototype is categorized as Port 2, as depicted in Fig. 10a.

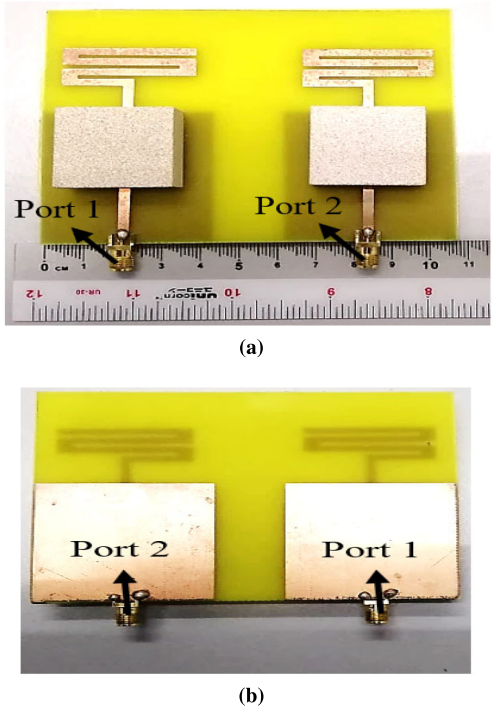

FIGURE 10. Prototype of the proposed MIMO hybrid DRA (a) 3D view (b) Back view.

Fig. 11 presents the simulated and measured S-parameters with reference levels of −15 dB for isolation and −10 dB on return loss for impedance bandwidth. The left SMA connector of the fabricated MIMO prototype is connected only to the coaxial cable that is linked to Port 1 of the Network Analyzer via an adapter to measure input return loss (S_{11}). The same

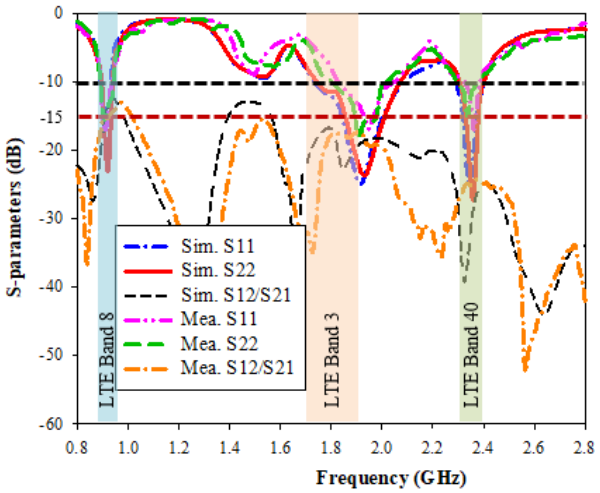

FIGURE 11. Simulated and measured S-parameters of the proposed MIMO hybrid DRA.

procedure is applied to Port 2 for measuring output return loss (S_{22}). Meanwhile, to measure isolation of the MIMO prototype, the left and right SMA connectors are connected to the coaxial cables that are linked to Ports 1 and 2 of the Agilent E5071C ENA Network Analyzer via adapters, respectively. With reference to Fig. 11, it can be observed that the measured and simulated bandwidths at 1.8 GHz for Ports 1 and 2 are slightly different. The simulated and measured impedance bandwidths are 18.93% (1.73-2.09 GHz) and 11.36% (1.83-2.05 GHz) at Port 1, and 17.39% (1.74-2.07 GHz) and 10.54% (1.80-2.00 GHz) at Port 2, respectively. However, the MIMO prototype has rather well-matched S-parameters at 0.9 GHz and 2.3 GHz. At 0.9 GHz, the simulated impedance bandwidth is the same as the measurement at each port, where 4.40% (0.89-0.93 GHz) is exhibited at Port 1 and 5.47% (0.89-0.94 GHz) at Port 2. Meanwhile, at 2.3 GHz, the simulated and measured impedance bandwidths are 4.69% (2.29-2.40 GHz) and 2.54% (2.33-2.39 GHz) at Port 1, and 4.26% (2.30-2.40 GHz) and 3.43% (2.29-2.37 GHz) at Port 2, respectively. Less than -15 dB of the measured isolation is also found within the bands of interest, which guarantees the maximum data rates.

Total radiation efficiencies for Ports 1 and 2 are calculated using Equations (6) and (7) [28] below. Comparisons between simulation and measurement for each antenna parameter is listed in Table 5, at the targeted frequencies for the proposed MIMO hybrid DRA. It can be observed from Table 5 that, the simulated and measured values of gain and total radiation efficiencies for both ports are similar.

$$\mu_{1,tot} = \mu_{1,rad}(1 - |S_{11}|^2 - |S_{21}|^2) \quad (6)$$

$$\mu_{2,tot} = \mu_{2,rad}(1 - |S_{22}|^2 - |S_{12}|^2) \quad (7)$$

Fig. 12 illustrates the measured and simulated normalized radiation patterns of E-plane and H-plane for both ports at each described frequency. Radiation patterns at Port 1 are obtained by exciting Port 1 of the MIMO prototype while

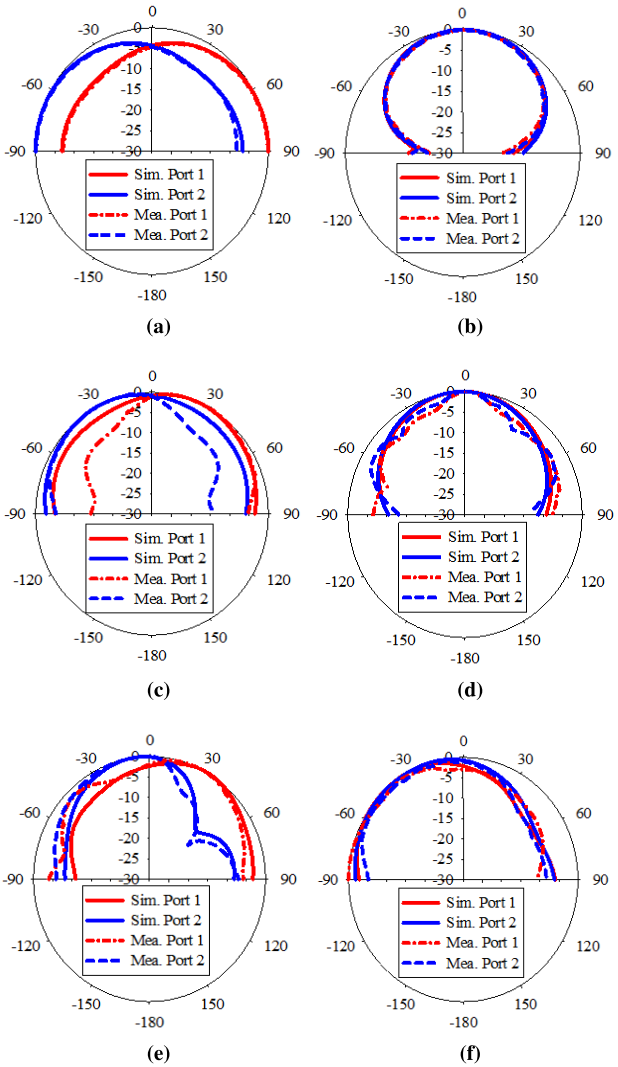

FIGURE 12. Measured and simulated normalized radiation patterns of the proposed MIMO hybrid DRA (a) E-Plane at 0.9 GHz (b) H-Plane at 0.9 GHz (c) E-Plane at 1.8 GHz (d) H-Plane at 1.8 GHz (e) E-Plane at 2.3 GHz (f) H-Plane at 2.3 GHz.

TABLE 5. Comparison between simulation and measurement of each antenna parameter for the proposed MIMO hybrid DRA.

Antenna Parameters			Freq. (GHz) 0.9	1.8	2.3
Covered BW. (%)	Port 1	Sim.	4.40	18.93	4.69
		Mea.	4.40	11.36	2.54
	Port 2	Sim.	5.47	17.39	4.26
		Mea.	5.47	10.54	3.43
Isolation (dB)		Sim.	-17.5	-16.9	-28.5
		Mea.	-15.3	-17.8	-47.0
Gain (dBi)	Port 1	Sim.	4.1	4.2	1.4
		Mea.	4.0	4.0	1.2
	Port 2	Sim.	4.1	4.0	2.0
		Mea.	3.9	3.9	1.8
Total Rad. Eff. (%)	Port 1	Sim.	74	69	60
		Mea.	70	65	58
	Port 2	Sim.	74	70	53
		Mea.	69	66	51

Port 2 is terminated by a load of 50Ω and vice versa for measuring radiation patterns at Port 2 [22]. Table 6 exhibits peak points of normalized radiation patterns for both Ports 1 and 2

TABLE 6. Peak points of normalized radiation patterns at each port for the proposed MIMO hybrid DRA.

Radiation patterns	Freq. (GHz)	Port 1	Port 2
E-plane	0.9	90°	-90°
	1.8	25°	-25°
	2.3	30°	-10°
H-plane	0.9	0°	0°
	1.8	0°	0°
	2.3	-30°	-25°

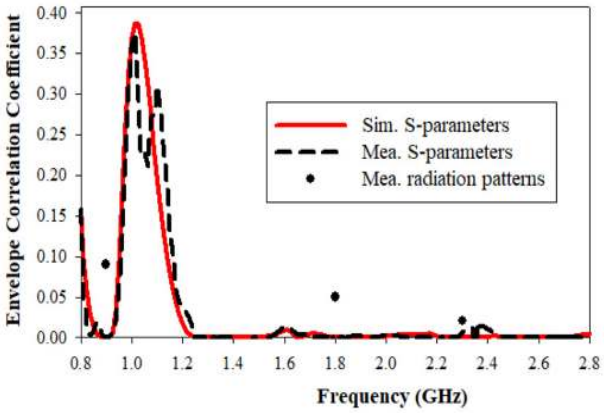

FIGURE 13. Simulated and measured Envelope Correlation Coefficient (ECC) of the proposed MIMO hybrid DRA.

of the proposed MIMO hybrid DRA. The performance in radiation patterns have some disagreements at 1.8 GHz for the proposed MIMO antenna, as shown in Fig. 12c and Fig. 12d. The potential causes are the same as mentioned previously for single port hybrid DRA.

C. MIMO PERFORMANCE ANALYSIS

The MIMO characteristic of the proposed MIMO antenna is assessed by Envelope Correlation Coefficient (ECC), Diversity Gain (DG), Mean Effective Gain (MEG) and Total Active Reflection Coefficient (TARC), to achieve multipath propagation [5].

Firstly, the Envelope Correlation Coefficient (ECC) is calculated by S-parameters using Equation (8) [29]. The simulated and measured ECC using S-parameters at the three stated frequencies is shown in Fig. 13. The measured values are 0.0005 at 0.9 GHz, 0.0003 at 1.8 GHz, and 0.0064 at 2.3 GHz, respectively. The results are inaccurate because the MIMO system is assumed to be operating in a uniform multipath environment [30]. Ideally, ECC is calculated by 3D radiation patterns [30] using Equation (9) [31] where $F_j^{\rightarrow}(\theta, \phi)$ is the normalized complex radiation pattern vector of the j^{th} port [32], and symbols . and * denote the Hermitian product and complex conjugate, respectively [33]. The measured 3D radiation patterns with a step of 1° using Equation (9) is 0.09, 0.05 and 0.02 at each mentioned frequency, respectively. In fact, ECC gives a correlation between signals at the receiving end [9]. Since the measured value of ECC using S-parameters and 3D radiation patterns at each

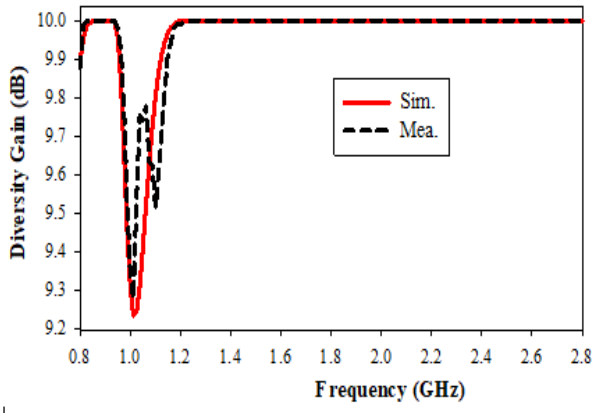

FIGURE 14. Simulated and measured Diversity Gain (DG) of the proposed MIMO hybrid DRA.

described frequency is less than 0.5 for mobile devices [34], the fading of the received signals is small [35]. Therefore, the proposed MIMO antenna is a good candidate for LTE applications.

$$\rho_e = \frac{|S_{11}^* S_{12} + S_{21}^* S_{22}|^2}{(1 - (|S_{11}|^2 + |S_{21}|^2))(1 - (|S_{22}|^2 + |S_{12}|^2))} \quad (8)$$

$$\rho_e = \frac{\left|\iint_{4\pi} F_1^{\rightarrow}(\theta, \phi) \cdot F_2^{\rightarrow *}(\theta, \phi) d\Omega\right|^2}{\left|\iint_{4\pi} F_1^{\rightarrow}(\theta, \phi) d\Omega\right|^2 \left|\iint_{4\pi} F_2^{\rightarrow}(\theta, \phi) d\Omega\right|^2} \quad (9)$$

Other than that, Diversity Gain (DG) is calculated to evaluate the MIMO performance of the proposed MIMO antenna using Equations (10) and (11) [1]. Diversity Gain is the amount of improvement obtained from a multiple antenna system relative to a single element system [36]. A comparison between the simulated and measured DG of the proposed MIMO antenna is depicted in Fig. 14. The measured values are 10 dB, 9.9999 dB, and 9.9997 dB at the three described frequencies, respectively. Since the measured value of DG in the desired frequency band is nearly at the maximum value of 10 dB [37], it indicates that a maximum improvement can be obtained by having the proposed MIMO system [36].

$$DG = 10 e_\rho \quad (10)$$

$$e_\rho = \sqrt{1 - |0.99 \rho_e|^2} \quad (11)$$

The Mean Effective Gain (MEG) performance is verified to test the MIMO performance of the proposed MIMO antenna. MEG is defined as the ratio of average power received at the antenna to the sum of average power of the vertically and horizontally polarized waves received by an isotropic antenna [9]. MEG for each port is calculated by S-parameters using Equation (12), whilst power ratio (k) which is the difference in the magnitude of MEGs, is calculated using Equation (13), where M is the total number of antennas [38]. The measured values at each described frequency are 0.0103 dB, 0.8339 dB, and 1.4735 dB, respectively. With reference to Fig. 15, it clearly indicates that there is no significant difference between the average power

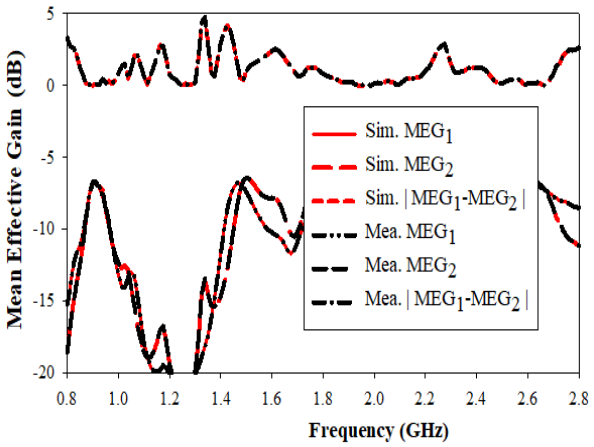

FIGURE 15. Simulated and measured Mean Effective Gain (MEG) of the proposed MIMO hybrid DRA.

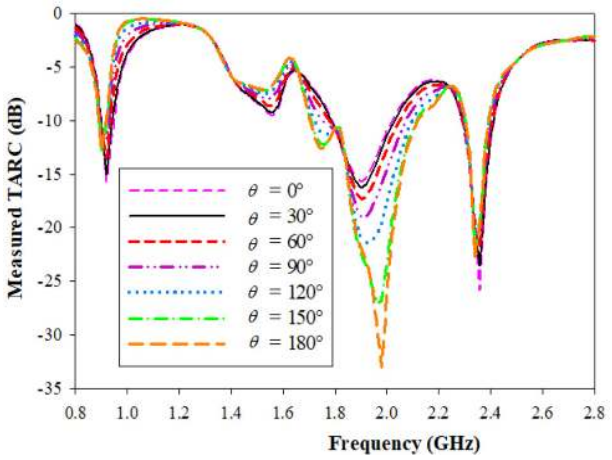

FIGURE 16. Measured TARC of the proposed MIMO DRA with θ ranging.

received at the prototype of MIMO antenna compared to the isotropic antenna, since the measured value of k is almost equal to 0 dB at the described frequency bands [9].

$$MEG_i = 0.5\eta_{i,rad} = 0.5\left[1 - \sum_{j=1}^{M} |S_{ij}|^2\right] \quad (12)$$

$$k = |MEG_1 - MEG_2| < 3dB \quad (13)$$

The Total Active Reflection Coefficient (TARC) is the last and very important parameter to be analyzed for diversity performance. It is used instead of the traditional scattering matrix, because the scattering matrix does not accurately characterize the radiating efficiency and bandwidth of an antenna array [39]. TARC is presented for multiport systems where it takes into consideration the effect when ports of the multiple antenna system are fed with random phases of return signal signals, which ranging from 0° to 180° with the steps of 30° [8]. It is because the reflected signal is assumed to be of unity magnitude, but randomly phased with Gaussian random variable since MIMO channels are assumed as Gaussian and exhibit a multipath spread in the propagation channel [40]. TARC is calculated using Equation (14) where θ is the phase difference between two feeding ports [41]. The measured TARC of the proposed MIMO DRA is shown in Fig. 16. It can be noticed that the proposed MIMO DRA always covers a triple band in the variation of the θ and follows the original behavior of the antenna characteristics.

$$\Gamma_a^t = \frac{\sqrt{(|S_{11} + S_{12}e^{j\theta}|^2) + (|S_{21} + S_{22}e^{j\theta}|^2)}}{\sqrt{2}} \quad (14)$$

D. THROUGHPUT PERFORMANCE ANALYSIS

The performance of the proposed MIMO antenna is further evaluated using an over-the-air LTE throughput test. Fig. 17 shows the throughput measurement setup of the proposed MIMO antenna. Downlink throughput is measured in bits per second (bps) to capture the amount of data transferred

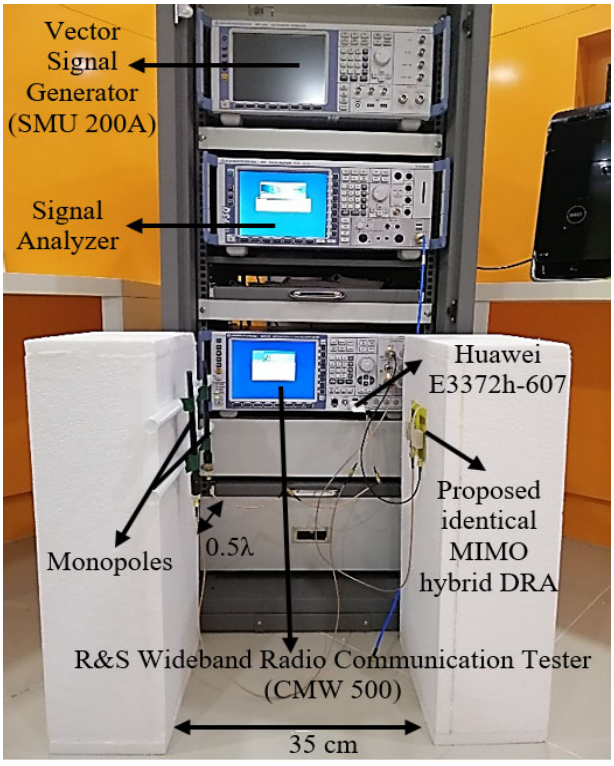

FIGURE 17. Throughput measurement setup of the proposed MIMO hybrid DRA.

wirelessly from the LTE eNodeB to the user equipment [9]. The theoretical maximum throughput has been referred to the capacity of the wireless link [42].

Throughput measurements and procedures presented in [9] have been referred to in this research work. Fig. 17 shows that the proposed triple band MIMO antenna has been placed with a separation distance of 35 cm from two monopoles (separated by 0.5λ spacing) in order to operate in the far-field region. The proposed MIMO antenna is connected to a Wideband Radio Communication Tester R&S° CMW500, which

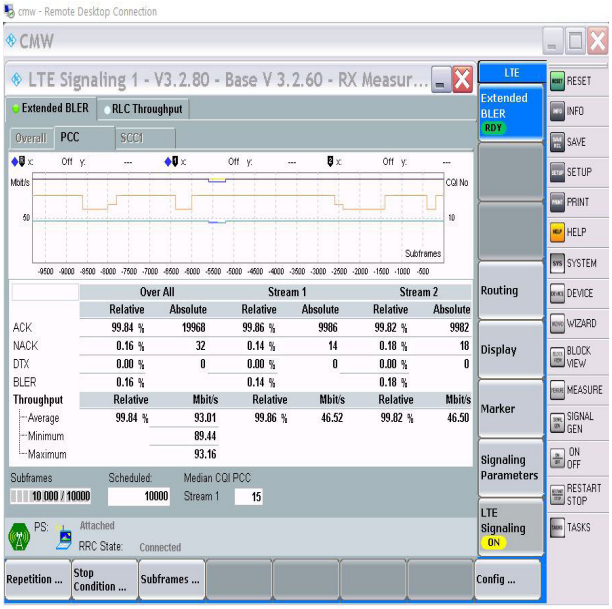

FIGURE 18. The theoretical maximum and the actual average measured throughput for 2 × 2 MIMO system with 64 QAM at 1.8 GHz (LTE Band 3) (as an example).

functions as an LTE base station (eNodeB) emulator, while the monopoles are connected to the antenna port of a Huawei E3372h-607 USB modem dongle, which functions as the LTE user equipment (UE). The eNodeB emulator transmits downlink data to the UE using the dedicated physical downlink shared channel subframes [9]. The positive and negative acknowledgements returned by UE are used to determine Block Error Rate (BLER) [9]. BLER is used in calculating the downlink throughput. Three types of modulations including QPSK (Quadrature Phase-shift Keying), 16 QAM (Quadrature Amplitude Modulation), and 64 QAM are utilized in this work. The parameters used in the measurement setup are, a bandwidth of 20 MHz, 100 resource blocks, −15 dBm of transmitted power, frequency bands at 0.9 GHz (LTE Band 8), 1.8 GHz (LTE Band 3), and 2.3 GHz (LTE Band 40), respectively. Other than that, at 2.3 GHz, uplink-downlink of Time Division Duplex (TDD) is set to configuration 5 in order to obtain the maximum downlink throughput.

Fig. 18 shows the measured throughput for a 2 × 2 MIMO system of the proposed MIMO antenna with 64 QAM at 1.8 GHz (LTE Band 3). The measured throughput of Streams 1 and 2 is 46.52 Mbps (light blue line) and 46.50 Mbps (moderate blue line), respectively. Meanwhile, the theoretical maximum throughput of 93.16 Mbps is represented by the yellow line, whereas the minimum measured throughput is 89.44 Mbps (orange line) and the actual average measured throughput is 93.01 Mbps (dark blue) in reference to Fig. 18. Tables 7, 8, and 9 display the theoretical maximum and the actual average measured throughput for the SISO and 2 × 2 MIMO systems of the presented MIMO antenna for the three modulation schemes along with the specific channel quality indicator (CQI) at each described

TABLE 7. The theoretical maximum and the actual average measured throughput for SISO and MIMO systems of the proposed MIMO hybrid DRA at 0.9 GHz (LTE Band 8).

Modulation Scheme (CQ1)	Throughput SISO (Mbps)		Throughput MIMO (Mbps)	
	Maximum	Measured	Maximum	Measured
QPSK (6)	14.112	14.11	28.224	28.22
16 QAM (9)	30.352	30.35	56.672	56.67
64 QAM (12)	50.197	50.19	93.162	93.16

TABLE 8. The theoretical maximum and the actual average measured throughput for SISO and MIMO systems of the proposed MIMO hybrid DRA at 1.8 GHz (LTE Band 3).

Modulation Scheme (CQ1)	Throughput SISO (Mbps)		Throughput MIMO (Mbps)	
	Maximum	Measured	Maximum	Measured
QPSK (6)	14.112	14.11	28.224	28.22
16 QAM (9)	30.352	30.35	56.672	56.67
64 QAM (12)	50.197	50.13	93.162	93.01

TABLE 9. The theoretical maximum and the actual average measured throughput for SISO and MIMO systems of the proposed MIMO hybrid DRA at 2.3 GHz (LTE Band 40).

Modulation Scheme (CQ1)	Throughput SISO (Mbps)		Throughput MIMO (Mbps)	
	Maximum	Measured	Maximum	Measured
QPSK (6)	12.319	12.31	24.638	24.63
16 QAM (9)	26.529	26.52	53.058	53.05
64 QAM (12)	43.662	43.66	87.324	87.30

frequency, respectively. The presented MIMO antenna manages to achieve around 99% of the theoretical maximum throughput of SISO and MIMO systems for all three listed modulation schemes at 0.9 GHz, 1.8 GHz, and 2.3 GHz, respectively. The 2 × 2 MIMO system has superior performance as it provides almost double the throughput compared to the SISO system, regardless of modulation schemes and frequencies. Undoubtedly, all the results analyzed in this work clearly indicate that the proposed identical MIMO hybrid DRA is suitable for LTE applications due to its delivery of excellent throughput performance of the 2 × 2 MIMO system.

Table 10 lists the comparison of simulated antenna parameters in terms of average bandwidth, gain, and total radiation efficiencies between the proposed MIMO design and existing structures. Based on the observations from Table 10, it can be inferred that the meander line which resonates at 0.9 GHz with merging DRA, has not been designed yet for LTE applications. Firstly, the proposed meander line antenna has a wider coverage area by having resonance at 0.9 GHz, compared to the antennas designed in [9], [22], [24]–[26], and [43]. Additionally, the proposed meander line with DRA has wider bandwidth performance, higher gain, and higher radiation efficiency at 1.8 GHz, compared to the antenna which is presented in [44]. Moreover, the proposed triple band meander line with DRA has more selections of frequency switching as compared to a single band antenna in [43] and a dual-band antenna in [9], for LTE applications. Lastly,

TABLE 10. Comparison of simulated antenna parameters between the proposed MIMO antenna and existing structures.

Year [Ref.]	Modifications on microstrip line	Total DRA used	Freq. (GHz)	MIMO	S_{12} (dB)	S_{11} Ref. (dB)	Average BW. (%)	Average Gain (dBi)	Average Total Rad. Eff. (%)
2015 [24]	Outer and inner triangular-shaped microstrip line	One CDRA	2.60 3.20 5.37	No	-	-10	4.90 19.23 17.57	2.0 2.5 5.0	Not stated
2018 [25]	A rectangular ring slot fed by microstrip line	One RDRA	1.80 2.60 3.40	No	-	-6	21.90 24.60 23.30	Not stated	Not stated
2016 [26]	Trapezoidal patch microstrip feed	One ring RDRA	2.40 5.00	No	-	-10	12.42 13.00	4.9 5.9	Not stated
2016 [22]	Folded microstrip line and two inverted L-shaped metallic strips	Two CDRAs	2.30 2.85 6.30	Yes	-15.0 -33.0 -35.0	-6	6.06 26.40 35.70	0.8 1.0 2.4	80.0 85.0 92.0
2017 [9]	Symmetrical slots coupled through microstrip feed lines	One L-shaped RDRA	1.80 2.60	Yes	-19.0 -38.0	-10	18.00 8.00	5.5 5.4	94.4 96.0
2015 [43]	Microstrip feed lines	Two RDRAs	1.80	Yes	-17.0	-6	26.38	3.2	Not stated
2016 [44]	Meander-line-type inverted-L	-	0.90 1.80 2.60	Yes	-11.0 -20.0 -25.0	-10	4.45 1.11 6.71	0.3 0.6 3.3	21.2 49.2 75.0
Proposed design	Meander line	Two RDRAs	0.90 1.80 2.30	Yes	-17.5 -16.9 -28.5	-10	4.40 18.93 4.69	4.1 4.2 1.4	74.0 69.0 60.0

the two proposed ports of the triple band meander line with DRA which can provide greater data rates, and are superior to the other antennas in [24]–[26] that have been designed for a single port only. The presented antenna parameters in Table 10 shows that the proposed MIMO antenna which has a triple band characteristic, is efficient and provides satisfactory performances for LTE applications.

IV. CONCLUSION

A triple band MIMO rectangular DRA designed using hybrid technique for LTE applications is proposed in this paper. The MIMO prototype manages to achieve −10 dB on return loss for impedance bandwidth and −15 dB of isolation at three different low, middle, and high frequency bands. There is a good agreement between the measured and simulated HFSS results in terms of S-parameters, gains, radiation efficiencies, and radiation patterns. Moreover, the measured value of ECC is less than 0.5, the measured value of DG is near to 10 dB, and the measured value of k is almost equal to 0 dB within the bands of interest, indicating that a good MIMO performance can be exhibited by the MIMO prototype. In addition to this, all the results presented in this work clearly indicate that the proposed identical MIMO hybrid DRA is suitable for LTE applications due to its delivery of an excellent throughput performance of the 2 × 2 MIMO system. This research can be extended by improving the mutual coupling between the two antenna ports to reduce the overall size of the MIMO system [2], to improve its radiation efficiency and for delivering higher data rates [45]. The interesting techniques are that, metamaterial spiral S-shaped resonators are applied between the two antenna ports [8], a metal strip is pasted on the upper surface of each DRA [41] and slots are cut through the ground plane [46], for parallel configuration.

REFERENCES

[1] S. F. Roslan, M. R. Kamarudin, M. Khalily, and M. H. Jamaluddin, "An MIMO rectangular dielectric resonator antenna for 4G applications," *IEEE Antennas Wireless Propag. Lett.*, vol. 13, pp. 321–324, 2014.

[2] I. Messaoudene, T. A. Denidni, and A. Benghalia, "CDR antenna with dual-band 1.9/2.7 GHz for MIMO-LTE terminals," *Microw. Opt. Technol. Lett.*, vol. 57, no. 10, pp. 2388–2391, 2015.

[3] Y.-L. Ban, C. Li, C.-Y.-D. Sim, G. Wu, and K.-L. Wong, "4G/5G multiple antennas for future multi-mode smartphone applications," *IEEE Access*, vol. 4, pp. 2981–2988, 2016.

[4] Y. M. Pan, K. W. Leung, and K. M. Luk, "Design of the millimeter-wave rectangular dielectric resonator antenna using a higher-order mode," *IEEE Trans. Antennas Propag.*, vol. 59, no. 8, pp. 2780–2788, Aug. 2011.

[5] Y. Ding, Z. Du, K. Gong, and Z. Feng, "A novel dual-band printed diversity antenna for mobile terminals," *IEEE Trans. Antennas Propag.*, vol. 55, no. 7, pp. 2088–2096, Jul. 2007.

[6] S. F. Roslan, M. R. Kamarudin, M. Khalily, and M. H. Jamaluddin, "An MIMO F-shaped dielectric resonator antenna for 4g applications," *Microw. Opt. Technol. Lett.*, vol. 57, no. 12, pp. 2931–2936, 2015.

[7] M. S. Sharawi, S. S. Iqbal, and Y. S. Faouri, "An 800 MHz 2 × 1 compact MIMO antenna system for LTE handsets," *IEEE Trans. Antennas Propag.*, vol. 59, no. 8, pp. 3128–3131, Aug. 2011.

[8] Y. Torabi and R. Omidi, "Novel metamaterial compact planar MIMO antenna systems with improved isolation for WLAN application," *Wireless Pers. Commun.*, vol. 102, no. 1, pp. 399–410, 2018.

[9] J. Nasir, M. H. Jamaluddin, A. A. Khan, M. R. Kamarudin, C. Y. Leow, and O. Owais, "Throughput measurement of a dual-band MIMO rectangular dielectric resonator antenna for LTE applications," *Sensors*, vol. 17, no. 1, p. 148, 2017.

[10] I. Nadeem and D.-Y. Choi, "Study on mutual coupling reduction technique for MIMO antennas," *IEEE Access*, vol. 7, pp. 563–586, 2019.

[11] R. Selvaraju, M. H. Jamaluddin, M. R. Kamarudin, J. Nasir, and M. H. Dahri, "Complementary split ring resonator for isolation enhancement in 5G communication antenna array," *Prog. Electromagn. Res. C*, vol. 83, pp. 217–228, Apr. 2018.

[12] K.-H. Chen and J.-F. Kiang, "Effect of mutual coupling on the channel capacity of MIMO systems," *IEEE Trans. Veh. Technol.*, vol. 65, no. 1, pp. 398–403, Jan. 2016.

[13] R. Selvaraju, M. H. Jamaluddin, M. R. Kamarudin, J. Nasir, and M. H. Dahri, "Mutual coupling reduction and pattern error correction in a 5G beamforming linear array using CSRR," *IEEE Access*, vol. 6, pp. 65922–65934, 2018.

[14] A. K. Sarangi and A. Datta, "Capacity comparison of SISO, SIMO, MISO & MIMO systems," in *Proc. 2nd Int. Conf. Comput. Methodol. Commun. (ICCMC)*, Erode, India, Feb. 2018, pp. 798–801.

[15] M. H. Jamaluddin, N. A. Mohammad, and S. Z. Naqiyah, "Size reduction of mimo dielectric resonator antenna for LTE application," in *Proc. IEEE Asia–Pacific Conf. Appl. Electromagn. (APACE)*, Langkawi, Malaysia, Dec. 2016, pp. 286–290.

[16] S. Keyrouz and D. Caratelli, "Dielectric resonator antennas: Basic concepts, design guidelines, and recent developments at millimeter-wave frequencies," *Int. J. Antennas Propag.*, vol. 2016, Sep. 2016, Art. no. 6075680.

[17] K. M. Luk and K. W. Leung, Eds., *Dielectric Resonator Antennas*. London, U.K.: Research Studies Press, 2003.

[18] B. Yousif, M. Sadiq, and M. Abdelrazzak, "Design and simulation of meander line antenna for LTE band," *Int. J. Sci. Eng. Res.*, vol. 6, no. 7, pp. 841–848, 2015.

[19] Y. Hong, J. Tak, J. Baek, B. Myeong, and J. Choi, "Design of a multiband antenna for LTE/GSM/UMTS band operation," *Int. J. Antennas Propag.*, vol. 2014, Jul. 2014, Art. no. 548160.

[20] D. Guha, A. Banerjee, C. Kumar, and Y. M. M. Antar, "New technique to excite higher-order radiating mode in a cylindrical dielectric resonator antenna," *IEEE Antennas Wireless Propag. Lett.*, vol. 13, pp. 15–18, 2014.

[21] H. M. Chen, Y. K. Wang, Y. F. Lin, S. C. Lin, and S. C. Pan, "A compact dual-band dielectric resonator antenna using a parasitic slot," *IEEE Antennas Wireless Propag. Lett.*, vol. 8, pp. 173–176, 2009.

[22] A. Sharma, G. Das, and R. K. Gangwar, "Dual polarized triple band hybrid MIMO cylindrical dielectric resonator antenna for LTE2500/WLAN/WiMAX applications," *Int. J. RF Microw. Comput. Aided Eng.*, vol. 26, no. 9, pp. 763–772, Nov. 2016.

[23] A. Sharma and R. K. Gangwar, "Compact dual-band ring dielectric resonator antenna with moon-shaped defected ground structure for WiMAX/WLAN applications," *Int. J. RF Microw. Comput.-Aided Eng.*, vol. 26, no. 6, pp. 503–511, 2016.

[24] A. Sharma and R. K. Gangwar, "Triple band hybrid cylindrical dielectric resonator antenna for WIMAX/WLAN applications," in *Proc. IEEE Appl. Electromagn. Conf. (AEMC)*, Guwahati, India, Dec. 2015, pp. 1–2.

[25] S. B. A. Rahim, C. K. Lee, A. Qing, and M. H. Jamaluddin, "A triple-band hybrid rectangular dielectric resonator antenna (RDRA) FOR 4G LTE applications," *Wireless Pers. Commun.*, vol. 98, no. 3, pp. 3021–3033, 2018.

[26] R. Selvaraju, M. Kamarudin, M. R. Khalily, J. Nasir, and M. Jamaluddin, "Dual band rectangular dielectric resonator antenna for WLAN application," *J. Teknologi*, vol. 78, nos. 2–6, pp. 65–69, 2016.

[27] N. Suleman and Rahmat, "Design of multiband MIMO 2 × 2 microstrip antenna with multi-slot method," *Int. J. Appl. Eng. Res.*, vol. 12, no. 19, pp. 8125–8130, 2017.

[28] G. P. Junker, A. A. Kishk, A. W. Glisson, and D. Kajifez, "Effect of air gap on cylindrical dielectric resonator antenna operating in TM_{01} mode," *Electron. Lett.*, vol. 30, no. 2, pp. 97–98, Jan. 1994.

[29] H. S. Singh, B. R. Meruva, G. K. Pandey, P. K. Bharti, and M. K. Meshram, "Low mutual coupling between MIMO antennas by using two folded shorting strips," *Prog. Electromagn. Res. B*, vol. 53, no. 10, pp. 205–221, 2013.

[30] J. Malik, D. Nagpal, and M. V. Kartikeyan, "Mimo antenna with omni-directional pattern diversity," *Electron. Lett.*, vol. 52, no. 2, pp. 102–104, 2016.

[31] Y. T. Wu and Q. X. Chu, "Dual-band multiple input multiple output antenna with slitted ground," *IET Microwaves, Antennas Propag.*, vol. 8, no. 13, pp. 1007–1013, Oct. 2014.

[32] K. Wang, R. A. M. Mauermayer, and T. F. Eibert, "Compact two-element printed monopole array with partially extended ground plane," *IEEE Antennas Wireless Propag. Lett.*, vol. 13, pp. 138–140, 2014.

[33] R. G. Vaughan and J. B. Andersen, "Antenna diversity in mobile communications," *IEEE Trans. Veh. Technol.*, vol. 36, no. 4, pp. 149–172, Nov. 1987.

[34] Y. Li, C.-Y.-D. Sim, Y. Luo, and G. Yang, "12-Port 5G massive MIMO antenna array in Sub-6GHz mobile handset for LTE bands 42/43/46 applications," *IEEE Access*, vol. 6, pp. 344–354, Oct. 2017.

[35] B. Feng, K. L. Chung, J. Lai, and Q. Zeng, "A conformal magneto-electric dipole antenna with wide H-plane and band-notch radiation characteristics for sub-6-GHZ 5G base-station," *IEEE Access*, vol. 7, pp. 17469–17479, 2019.

[36] J. Nasir, M. H. Jamaluddin, M. Khalily, M. R. Kamarudin, I. Ullah, and R. Selvaraju, "A reduced size dual port MIMO DRA with high isolation for 4G applications," *Int. J. RF Microw. Comput.-Aided Eng.*, vol. 25, no. 6, pp. 495–501, 2015.

[37] A. A. Khan, M. H. Jamaluddin, S. Aqeel, J. Nasir, J. ur Rehman Kazim, and O. Owais, "Dual-band MIMO dielectric resonator antenna for WiMAX/WLAN applications," *IET Microw., Antennas Propag.*, vol. 11, no. 1, pp. 113–120, Jan. 2017.

[38] L. F. Zou, D. Abbott, and C. Fumeaux, "Omnidirectional cylindrical dielectric resonator antenna with dual polarization," *IEEE Antennas Wireless Propag. Lett.*, vol. 11, pp. 515–518, 2012.

[39] M. Manteghi and Y. Rahmat-Samii, "Multiport characteristics of a wide-band cavity backed annular patch antenna for multipolarization operations," *IEEE Trans. Antennas Propag.*, vol. 53, no. 1, pp. 466–474, Jan. 2005.

[40] S. H. Chae, S.-K. Oh, and S.-O. Park, "Analysis of mutual coupling, correlations, and TARC in WiBro MIMO array antenna," *IEEE Antennas Wireless Propag. Lett.*, vol. 6, pp. 122–125, 2007.

[41] Y. Zhang, J.-Y. Deng, M.-J. Li, D. Sun, and L.-X. Guo, "A MIMO dielectric resonator antenna with improved isolation for 5G mm-Wave applications," *IEEE Antennas Wireless Propag. Lett.*, vol. 18, no. 4, pp. 747–751, Apr. 2019.

[42] A. Moradikordalivand, T. A. Rahman, C. Y. Leow, and S. Ebrahimi, "Dual-polarized MIMO antenna system for WiFi and LTE wireless access point applications," *Int. J. Commun. Syst.*, vol. 30, no. 1, p. e2898, 2017.

[43] R. Selvaraju, M. R. Kamarudin, M. Khalily, M. H. Jamaluddin, and J. Nasir, "Dual-port MIMO rectangular dielectric resonator antenna for 4G-LTE application," *Appl. Mech. Mater.*, vol. 781, no. 6, pp. 24–27, 2015.

[44] J.-S. Sun, H.-S. Fang, P.-Y. Lin, and C.-S. Chuang, "Triple-band MIMO antenna for mobile wireless applications," *IEEE Antennas Wireless Propag. Lett.*, vol. 15, pp. 500–503, 2016.

[45] L. Zhao and K.-L. Wu, "A dual-band coupled resonator decoupling network for two coupled antennas," *IEEE Trans. Antennas Propag.*, vol. 63, no. 7, pp. 2843–2850, Jul. 2015.

[46] S. Zuo, Y.-Z. Yin, W.-J. Wu, Z.-Y. Zhang, and J. Ma, "Investigations of reduction of mutual coupling between two planar monopoles using two λ/4 slots," *Prog. Electromagn. Res. Lett.*, vol. 19, no. 2, pp. 9–18, 2010.

IRENE KONG CHEH LIN received B.Eng. degree (Hons.) in electrical engineering (electronics) from Universiti Malaysia Pahang (UMP), Malaysia, in 2016, and the master's degree in electronics and communication engineering from Universiti Teknologi Malaysia (UTM), Malaysia, in 2018, where she is currently pursuing the Ph.D. degree with the Wireless Communication Centre (WCC), School of Electrical Engineering. Her research interests include dielectric resonator antennas and MIMO antennas.

MOHD HAIZAL JAMALUDDIN received the bachelor's and master's degrees in electrical engineering from Universiti Teknologi Malaysia (UTM), Malaysia, in 2003 and 2006, respectively, and the Ph.D. degree in signal processing and telecommunications from the Université de Rennes 1, France, in 2009, with a focus on microwave communication systems and specially antennas, such as dielectric resonator and reflectarray and dielectric dome antennas. He is currently an Associate Professor with the Wireless Communication Centre, School of Electrical Engineering, UTM. He has published more than 100 articles in reputed indexed journals and conference proceedings. His research interests include dielectric resonator antennas, printed microstrip antennas, MIMO antennas, and DRA reflectarray antennas.

AZLAN AWANG (SM'16) received the B.Sc. and M.Sc. degrees in electrical engineering from the Polytechnic Institute of NYU (now NYU Tandon School of Engineering), Brooklyn, NY, USA, in 1989 and 1990, respectively, and the Ph.D. degree from IMT Atlantique/Télécom Bretagne and University Rennes 1, Rennes, France, in 2011. He was with various multinational companies, including Motorola (M) Sdn Bhd, in 1991, Schlumberger Overseas S.A., from 1992 to 1993, and Alcatel Networks Systems (M) Sdn Bhd, from 1994 to 2001. From 2002 to 2003, he was with Universiti Teknologi MARA. In 2004, he joined Universiti Teknologi PETRONAS (UTP), Malaysia, and has served as the Cluster Head for computer and communication (C&C) cluster at the Department of Electrical and Electronic Engineering, from 2013 to 2016. He is currently with the Center for Smart Grid Energy Research (CSMER), Institute of Autonomous System, UTP. His research interests include the design of energy-efficient, cross-layer medium access control and routing protocol in vehicular ad hoc networks, wireless sensor networks, and wireless body area networks. He is also a member of the IEEE Eta Kappa Nu and Tau Beta Pi Engineering Honor Societies and a Chartered Engineer with Engineering Council, U.K. He received one of the two Best Paper Awards in MICC2013 (20 years of MICC, from 1993 to 2013).

RAGHURAMAN SELVARAJU was born in Gandarvakottai, India, in 1989. He received the bachelor's degree in electronics and communication engineering and the master's degree in wireless communication systems from Periyar Maniammai University, India, in 2011 and 2014, respectively. He is currently pursuing the Ph.D. degree with the Wireless Communication Centre (WCC), School of Electrical Engineering, Universiti Teknologi Malaysia (UTM), Malaysia. His research interests include microstrip patch antennas, dielectric resonator antennas, MIMO antennas, beamforming array antennas, mutual coupling analysis, metamaterials, and split-ring resonators.

MUHAMMAD HASHIM DAHRI received the B.E. degree in telecommunications from the Mehran University of Engineering and Technology (MUET), Pakistan, in 2010, the master's by research degree in electrical engineering from Universiti Tun Hussein Onn Malaysia (UTHM), in 2014, and the Ph.D. degree from the Wireless Communication Centre (WCC), Universiti Teknologi Malaysia (UTM), in 2019. He is currently a Postdoctoral Research Fellow with UTHM. He has authored over 25 research articles in various indexed journals and conference proceedings. His research interests include reflectarray antennas, planar printed antennas, and tunable materials for antenna design.

LEOW CHEE YEN (S'08–M'12) received the B.Eng. degree in computer engineering from Universiti Teknologi Malaysia (UTM), Johor Bahru, Malaysia, in 2007, and the Ph.D. degree from the Imperial College London, U.K., in 2011. Since July 2007, he has been an Academic Staff with the School of Electrical Engineering, Faculty of Engineering, UTM. He is currently an Associate Professor with the Faculty and a Research Fellow in the Wireless Communication Centre (WCC), Higher Institution Centre of Excellence, UTM, and the UTM-Ericsson Innovation Centre for 5G. His research interests include non-orthogonal multiple access, cooperative communication, UAV communication, MIMO, hybrid beamforming, physical layer security, wireless power transfer, convex optimization, game theory, and prototype development using software-defined radio for the 5G and the IoT applications.

HASLIZA A. RAHIM received the bachelor's degree in electrical engineering from the University of Southern California, Los Angeles, CA, USA, in 2003, the master's degree in electronics design system from Universiti Sains Malaysia, Malaysia, in 2006, and the Ph.D. degree in communication engineering from Universiti Malaysia Perlis (UniMAP), Perlis, Malaysia, in 2015. In 2006, she joined the School of Computer and Communication Engineering (SCCE), UniMAP, as a Lecturer, where she is currently a Senior Lecturer. She is also the Programme Chairperson for postgraduate studies at SCCE, UniMAP. She is also a Researcher with the Bioelectromagnetics Research Group, SCCE. She was leading the Malaysian Communications and Multimedia Commission Research Grant (worth U.S. $150k). She has been mentoring several undergraduate and about 12 graduate students. She has authored or coauthored about 100 leading international technical journal and peer-reviewed conference articles, including three articles in Nature Publishing Group journals (Scientific Reports), three patents, and two book chapters. Her research interests include wearable and conformal antennas, metamaterials, antenna interaction with human body, on-body communications, green microwave absorbers, wireless body area networks, bioelectromagnetics, physical layer protocols for WBAN, and 5G massive multiple input-multiple output systems. Several research funds were granted nationally and internationally, such as the Fundamental Research Grant Scheme, the National Science Fund, and the Short Term Grant of UOWD (worth U.S. $375k). She has been a member of the technical program committees of several IEEE conferences and technical reviewer for several IEEE and other conferences. She is also a member of the IET and IEEE MTT-S and a Graduate Member of the Board of Engineers Malaysia. As an Advisor, her supervised projects have also won prizes, such as the Third Place in IEEE Malaysia Section Final Year Project Competition (Telecommunication Track), in 2017. She was recognized as the Excellence Woman Inventor by UniMAP, in 2011. She received the Silver medal at the International Invention, Innovation and Technology Exhibition (ITEX 2018).